

Generic long-range interactions between passive bodies in an active fluid

Yongjoo Baek,¹ Alexandre P. Solon,² Xinpeng Xu,¹ Nikolai Nikola,¹ and Yariv Kafri¹

¹*Department of Physics, Technion – Israel Institute of Technology, Haifa 32000, Israel*

²*Department of Physics, Massachusetts Institute of Technology, Cambridge, Massachusetts 02139, USA*

(Dated: April 19, 2023)

A single non-spherical body placed in an active fluid generates currents. We show that when two or more passive bodies are placed in an active fluid these currents lead to long-range interactions. Using a multipole expansion we characterize their leading-order behaviors in terms of single-body properties and show that they decay as a power law with the distance between the bodies, are anisotropic, and do not obey an action–reaction principle. The interactions lead to rich dynamics of the bodies, illustrated by the spontaneous synchronized rotation of pinned non-chiral bodies and the formation of traveling bound pairs. The occurrence of these phenomena depends on tunable properties of the bodies, thus opening new possibilities for self-assembly mediated by active fluids.

Active matter is a class of nonequilibrium systems in which energy is converted into systematic motion on a microscopic scale [1]. They have attracted much attention [2, 3] due to a host of interesting physical phenomena [4–9], their relevance to many biological systems [10–13], and their potential use for self-assembly applications [14]. They have also been suggested as tools for novel engineering applications – for example, active fluids have been used to power microscopic gears [15–21]. This is a direct consequence of the fact that when an asymmetric body is immersed in a fluid which breaks time-reversal symmetry it experiences a net force [22, 23] which is coupled to the generation of ratchet-like currents [24–26].

In this article we study passive bodies immersed in an active fluid. We show that the ratchet-like currents generated by each body give rise to forces and torques which decay as a power law with distance, are anisotropic, and do not obey an action–reaction principle. Using a multipole expansion, the leading-order behavior of the interactions can be expressed in terms of single-body quantities that can be measured independently in experiments or numerical simulations. Moreover, by designing the two bodies one can control the amplitude and polarity of the interactions between them. This leads to a host of interesting dynamical phenomena of which we illustrate two: the spontaneous synchronized rotations of pinned rotors and the formation of traveling bound pairs. Our results suggest a new method for self-assembly by embedding passive bodies in an active fluid.

We stress that the interactions studied here exist even between non-moving bodies and are therefore distinct from usual hydrodynamic interactions [27]. They are also different from thermal Casimir interactions which result from long-range correlations inside a fluid [28, 29]. The interactions do not rely on correlations between the fluid particles and are present even in a dilute active fluid.

Model. — We base our study on a common model of an active fluid consisting of N point-like noninteracting particles, self-propelled at a constant speed v in two dimensions. The position \mathbf{r}_i and the orientation θ_i of active particle i evolve according to the overdamped Langevin

equations

$$\begin{aligned}\dot{\mathbf{r}}_i &= v\mathbf{e}_{\theta_i} - \mu \sum_j \nabla V_j + \sqrt{2D_t}\boldsymbol{\eta}_i, \\ \dot{\theta}_i &= \sqrt{2D_r}\xi_i.\end{aligned}\quad (1)$$

Here $\mathbf{e}_{\theta_i} \equiv (\cos \theta_i, \sin \theta_i)$ is the heading of particle i , μ is its mobility, V_j is a potential describing body j , D_t and D_r are translational and rotational diffusivities, and $\boldsymbol{\eta}_i$ and ξ_i are Gaussian white noises of unit variance. The dots denote derivatives with respect to time. In addition, we allow the particles to randomize their orientation at a constant tumbling rate α . This dynamics encompass the two well-studied models of run-and-tumble particles (RTPs, with $\alpha \neq 0$ and $D_r = 0$) [30] and active Brownian particles (ABPs, having $\alpha = 0$ and $D_r \neq 0$) [31, 32]. There has been much recent progress [23, 25, 33–46] in the characterization of forces in this class of systems and we build upon it. Note that the model falls into the class of dry active systems, which do not conserve momentum. As such it is best suited for describing the dynamics of particles next to a surface, for example those of vibrated granular monolayers [47–49] or gliding bacteria [50].

A single passive body. — Before turning to interacting bodies we first consider a passive body j in an active fluid. Using standard methods [51, 52] (detailed for completeness in Appendix B), Eq. (1) can be used to obtain an exact equation for the particle density ρ_j in the steady state

$$D_{\text{eff}}\nabla^2\rho_j = -\mu\nabla\cdot(\rho_j\nabla V_j) + \sum_{a,b}\partial_a\partial_b(\mathbb{G}_j)_{ab}.\quad (2)$$

Here $D_{\text{eff}} \equiv D_t + v l_r/2$ is the effective diffusion constant of the active particles, $l_r \equiv v/(\alpha + D_r)$ their run length, indices a and b run over the Cartesian coordinates $\{x, y\}$, and \mathbb{G}_j is a rank 2 tensor. In the far-field limit (at distances r much larger than the microscopic length scales, *i.e.* the diameter of the body and the run length l_r), the solution of Eq. (2) can be written to dipole order in a

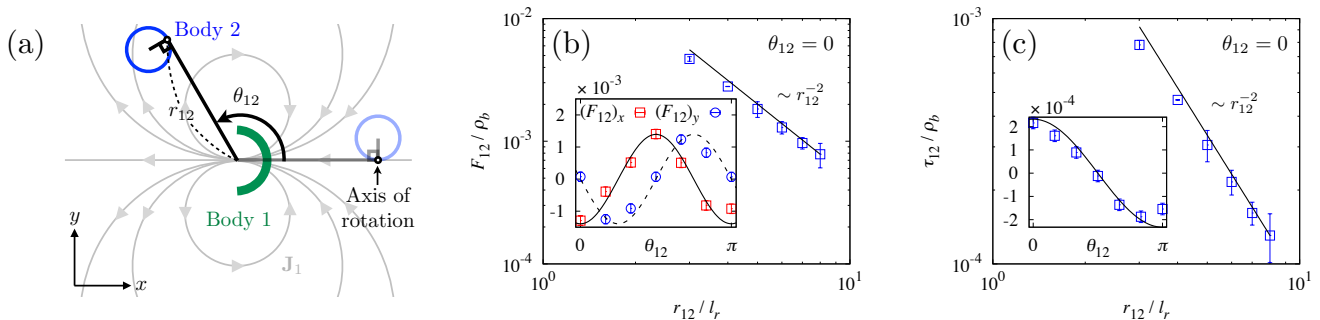


FIG. 1. Dipole contributions to far-field interactions. (a) The numerical setup used to verify the theoretical predictions. A circular body is placed at different distances r_{12} and angles θ_{12} away from a semicircular body which generates a dipole current. (b) The force normalized by the bulk density as a function of r_{12}/l_r , with l_r the run length, for $\theta_{12} = 0$. (Inset) The dependence of the force components $(F_{12})_{x,y}$ in the x - and y -directions as a function of θ_{12} . (c) The torque applied by the semicircle on a circle which is held tangent to \mathbf{r}_{12} and pinned at the contact point as θ_{12} is varied, see (a). The lines in (b) and (c) correspond to the theory with no fitting parameters. All the parameters and units of the simulations are specified in Appendix A 4.

multipole expansion as

$$\rho_j(\mathbf{r}) = \rho_b + \frac{\beta_{\text{eff}}}{2\pi} \frac{\mathbf{r} \cdot \mathbf{p}_j}{r^2} + O(r^{-2}), \quad (3)$$

where ρ_b denotes the bulk density of active particles and $\beta_{\text{eff}} \equiv \mu/D_{\text{eff}}$ their effective inverse temperature. The dipole moment \mathbf{p}_j of body j is given by

$$\mathbf{p}_j = - \int d^2\mathbf{r}' \rho_j \nabla' V_j. \quad (4)$$

It is equal to the total force exerted by body j on the active particles, or alternatively, $-\mathbf{p}_j$ is the propulsion force applied by the active particles on body j . As previously noted, it is nonzero for asymmetric bodies due to ratchet-like effects. We stress that at this order Eqs. (3) and (4) are exact, with \mathbb{G}_j in Eq. (2) only contributing to higher-order multipoles. The value of \mathbf{p}_j can be easily measured in numerical simulation but is difficult to predict analytically because it depends on the details of the density profile close to the body. However, we show in Appendix E that it can be computed perturbatively for shallow potentials $\beta_{\text{eff}}|\nabla V_j| \ll 1$.

The associated far-field current density is dominated by the diffusive component

$$\mathbf{J}_j(\mathbf{r}) \simeq -D_{\text{eff}} \nabla \rho_j \simeq -\frac{\mu}{2\pi} \left[\frac{\mathbf{p}_j}{r^2} - \frac{2(\mathbf{r} \cdot \mathbf{p}_j)\mathbf{r}}{r^4} \right]. \quad (5)$$

The pattern of the current flow is thus identical to the electric field of a charge dipole. In addition, it is easy to verify that $\mu\mathbf{p}_j = \int d^2\mathbf{r} \mathbf{J}_j$, as shown more generally for this class of models in [25]. The form of the density and current shows that the potential acts as a local pump in a diffusive medium, studied in [53].

Forces between passive bodies. — We now consider two passive bodies described by potentials V_1 and V_2 , with dipole moments (in isolation) \mathbf{p}_1 and \mathbf{p}_2 , and position

vectors \mathbf{R}_1 and \mathbf{R}_2 . We set $\mathbf{R}_2 = 0$ and $\mathbf{R}_1 = \mathbf{r}_{12}$ and work in the far-field limit where $r_{12} = |\mathbf{r}_{12}|$ is much larger than the run length l_r and the diameters of the bodies. We define the force applied by body 1 on body 2, denoted by \mathbf{F}_{12} , as the change in the force acting on body 2 due to the presence of body 1 ($\mathbf{F}_{12} - \mathbf{p}_2$ is then the total force acting on body 2). The force \mathbf{F}_{12} results from changes in the density field near body 2 due to the presence of body 1. It can be obtained as a power-series in r_{12}^{-1} (see Appendix C 1 for a detailed derivation). It is convenient to separate the total force into two components $\mathbf{F}_{12} = \mathbf{F}_{12}^{\text{non-sym}} + \mathbf{F}_{12}^{\text{sym}}$: $\mathbf{F}_{12}^{\text{non-sym}}$ acts only on asymmetric bodies with nonzero \mathbf{p}_j , while $\mathbf{F}_{12}^{\text{sym}}$ is present even for symmetric bodies with $\mathbf{p}_j = 0$. We find

$$\mathbf{F}_{12}^{\text{non-sym}} = -\frac{\beta_{\text{eff}}}{2\pi\rho_b} \frac{\mathbf{r}_{12} \cdot \mathbf{p}_1}{r_{12}^2} \mathbf{p}_2 + O(r_{12}^{-2}), \quad (6)$$

$$\mathbf{F}_{12}^{\text{sym}} = \frac{\mathbb{R}_2 \mathbf{J}_1(\mathbf{r}_{12})}{\rho_b} + O(r_{12}^{-3}). \quad (7)$$

Here \mathbb{R}_2 is the inverse mobility tensor of body 2 due to the active particles. It is measured by dragging body 2 alone in an active fluid of bulk density ρ_b at velocity \mathbf{u} and calculating

$$(\mathbb{R}_2)_{ab} = \left. \frac{\partial}{\partial u_b} [\mathbf{F}_2(\mathbf{u}) \cdot \mathbf{e}_a] \right|_{\mathbf{u}=0}, \quad (8)$$

where indices a and b stand for Cartesian coordinates $\{x, y\}$, \mathbf{e}_a is a unit vector in the a -direction, and $\mathbf{F}_2(\mathbf{u})$ is the steady-state force on the body. Finally, \mathbf{J}_1 in Eq. (7) is given by Eq. (5). At this order, the interactions between the two bodies are thus completely determined by \mathbf{p}_1 , \mathbf{p}_2 , and \mathbb{R}_2 , which are single-body quantities that can be measured independently.

We can understand Eqs. (6) and (7) intuitively in terms of the density and current fields produced by body 1 alone. First, we note that body 2 by itself experiences a

propulsion force $-\mathbf{p}_2$ in the absence of body 1. Since the noninteracting active particles are independent of each other, the propulsion force is proportional to the bulk density ρ_b . With body 1 added its dipole density field changes the effective bulk density felt by body 2 from ρ_b to $\rho_1(\mathbf{r}_{12})$, given in Eq. (3). This leads to Eq. (6) with $\mathbf{F}_{12}^{\text{non-sym}} \sim r_{12}^{-1}$. Therefore $\mathbf{F}_{12}^{\text{non-sym}}$ only induces a correction to the speed of the body.

Meanwhile, $\mathbf{F}_{12}^{\text{sym}} \sim r_{12}^{-2}$ because it stems from the current field $\mathbf{J}_1(\mathbf{r}_{12})$ generated by body 1 in accordance with Eq. (5). Galilean invariance implies that the force experienced by a body in a uniform current field (for sufficiently large r_{12} , \mathbf{J}_1 is almost uniform across body 2) is equivalent to the force experienced by the same body traveling at velocity $\mathbf{u} = -\mathbf{J}_1/\rho_b$ through a static medium. Under conditions discussed in Appendix C2 the drag force can be linearized as $\mathbb{R}_2\mathbf{J}_1(\mathbf{r}_{12})/\rho_b$. Note that $\mathbf{F}_{12}^{\text{sym}}$ can change the propulsion direction of body 2. In Fig. 1 we present a measurement of the force \mathbf{F}_{12} on a circular body (so that $\mathbf{p}_2 = 0$). In this case \mathbb{R}_2 is proportional to the identity matrix and we evaluated it numerically. The results agree nicely with the theory using no fitting parameters, although on a reduced range because of numerical limitations.

Torques between passive bodies. — The torque $\boldsymbol{\tau}_{12}$ exerted by body 1 on body 2 can be obtained using the same approach. We denote by $\boldsymbol{\tau}_j = \int d^2\mathbf{r}' \rho_j(\mathbf{r}') (\mathbf{r}' - \mathbf{R}_j) \times \nabla' V_j$ the self-torque experienced by an isolated body j with respect to the reference position \mathbf{R}_j . It is useful to decompose the result into a correction to the self-torque $\boldsymbol{\tau}_{12}^{\text{non-sym}}$, which is dominant when $\boldsymbol{\tau}_2 \neq 0$, and a sub-leading contribution $\boldsymbol{\tau}_{12}^{\text{sym}}$, which can induce a torque even when $\boldsymbol{\tau}_2 = 0$. We find

$$\boldsymbol{\tau}_{12}^{\text{non-sym}} = \frac{\beta_{\text{eff}}}{2\pi\rho_b} \frac{\mathbf{r}_{12} \cdot \mathbf{p}_1}{r_{12}^2} \boldsymbol{\tau}_2 + O(r_{12}^{-2}), \quad (9)$$

$$\boldsymbol{\tau}_{12}^{\text{sym}} = \frac{\gamma_2}{\rho_b} \times \mathbf{J}_1(\mathbf{r}_{12}) + O(r_{12}^{-3}), \quad (10)$$

where the vector γ_2 , similarly to \mathbb{R}_2 , is a response coefficient obtained by dragging a single body in an active fluid of density ρ_b at velocity \mathbf{u} and measuring the steady-state torque, $\boldsymbol{\tau}_2(\mathbf{u})$, exerted on it

$$\boldsymbol{\gamma}_2 = -[\nabla_{\mathbf{u}} \times \boldsymbol{\tau}_2(\mathbf{u})]_{\mathbf{u}=0}. \quad (11)$$

As with Eqs. (6) and (7), $\boldsymbol{\tau}_{12}^{\text{non-sym}}$ results from a local shift in the density, while $\boldsymbol{\tau}_{12}^{\text{sym}}$ originates from the current. The latter tends to align $\boldsymbol{\gamma}_2$ with the local current. In Fig. 1, our predictions are compared with simulations which measure the torque exerted by a semicircle (body 1) on a circle (body 2) held at its edge, with $\boldsymbol{\gamma}_2$ evaluated numerically.

Note that the forces and torques between the bodies are anisotropic and do not obey an action–reaction principle. In addition, it is straightforward to show that when three or more bodies are well separated the dominating interactions arise from the pairwise interactions. The multipole expansion implies that two rods would inter-

act through quadrupole moments. This setup has been considered in [54] but only in the near field. We predict an additional long-range force decaying as r_{12}^{-3} . In Fig. 5 we present numerics consistent with these predictions. Finally, it is also straightforward to generalize the analysis to dimensions d larger than two. One then finds $\mathbf{F}_{12}^{\text{non-sym}} \sim r_{12}^{-(d-1)}$ and $\mathbf{F}_{12}^{\text{sym}} \sim r_{12}^{-d}$ with corresponding changes to the torques.

For bodies that are allowed to move in the fluid, the interactions can lead to a host of interesting dynamical phenomena. Assuming that the bodies are overdamped, we take

$$\begin{aligned} \dot{\mathbf{R}}_j &= \mu_j^T \int d^2\mathbf{r} \rho(\mathbf{r}, t) \nabla V_j, \\ \dot{\Theta}_j &= \mu_j^R \int d^2\mathbf{r} \rho(\mathbf{r}, t) [(\mathbf{r} - \mathbf{R}_j) \times \nabla V_j] \cdot \mathbf{e}_z, \end{aligned} \quad (12)$$

where μ_j^T and μ_j^R are the translational and rotational mobilities of body j , Θ_j is an angle giving its orientation with respect to a fixed axis of reference, and \mathbf{R}_j is a position vector. For simplicity we consider bodies for which the position vector \mathbf{R}_j can be chosen so that no off-diagonal mobilities couple the translational and rotational degrees of freedom. The extension to other cases is straightforward. The results derived above are applicable when the mobilities are small enough so that an adiabatic limit holds: at each instant, the system can be considered to be in a steady state with fixed body positions. We do not specify direct (short-range) interactions between the bodies since here we consider only far-field effects. Interestingly, we show that properties of the bodies can be tuned to lead to distinct phenomena.

For concreteness, we consider pairs of *semicircles*. A semicircle traps active particles approaching from the concave side (‘rear’), while those on the convex side (‘front’) easily slide past the body. This creates a backward current of active particles, associated with an opposing force [25] which propels the semicircle forward (see Fig. 1a). In the terminology introduced above, a semicircle has a nonzero dipole moment \mathbf{p}_j pointing in the backward direction. We focus on two types of semicircles that rotate around \mathbf{R}_j either at the apex (type *A*) or at the center of the circle (type *C*). In experiments, this could be achieved by properly designing the bodies. Most importantly for their dynamics, $\boldsymbol{\gamma}_j$ is parallel to \mathbf{p}_j for type *C* bodies and antiparallel for type *A* bodies. In both cases, \mathbf{R}_j is on the symmetry axis so that $\boldsymbol{\tau}_A = \boldsymbol{\tau}_C = 0$.

Spontaneous synchronized rotations of pinned rotors. — We consider a pair of semicircles, one type *A*, pinned to the surface at its apex, and one type *C*, pinned to the surface at its center. They are placed at a distance much larger than l_r so that we can understand their dynamics in terms of the far-field torques given in Eq. (10). The torques align $\boldsymbol{\gamma}_{A/C}$ with the current generated by the other circle, which depends only on the dipole moment, taken to be equal for both. To describe the dynamics we define two angles θ_C and θ_A as the orientation of $\boldsymbol{\gamma}_C$

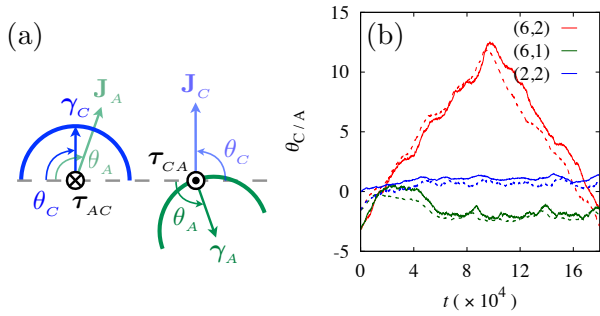


FIG. 2. Phase-locking and spontaneous rotations of pinned rotors. (a) An illustration of type C and type A semicircles pinned to the surface (not shown to scale). In the numerics the distance between the pinning points of the semicircles is $5l_r$. (b) The history of the angles θ_C (solid lines) and θ_A (dotted lines) for rotational mobilities given by (μ_C^R, μ_A^R) . In case (2, 2), the solid line indicates $\theta_C + \pi$ instead of θ_C . All the parameters and units of the simulations are specified in Appendix A 4.

and γ_A with respect to the horizontal, as represented in Fig. 2. Note that θ_C is defined with a clockwise convention and θ_A counterclockwise. Neglecting noise, we can write the dynamics of the angle difference $\theta_C - \theta_A$ in the adiabatic limit as

$$\begin{aligned} \dot{\theta}_C - \dot{\theta}_A &= \frac{1}{\rho_b} (\mu_C^R \tau_{AC} - \mu_A^R \tau_{CA}) \cdot \mathbf{e}_z \\ &= -\frac{\mu_C^R J_A \gamma_C - \mu_A^R J_C \gamma_A}{\rho_b} \sin(\theta_C - \theta_A), \end{aligned} \quad (13)$$

where $\gamma_j \equiv |\gamma_j|$, $J_j \equiv |\mathbf{J}_j|$. For $\mu_C^R J_A \gamma_C > \mu_A^R J_C \gamma_A$ the angles tend to phase-lock at $\theta_C = \theta_A$ while for $\mu_C^R J_A \gamma_C < \mu_A^R J_C \gamma_A$ they phase-lock at $\theta_C = \theta_A + \pi$. Using this we can expand in small deviations from the locking angle difference. The equation for θ_A then reduces to

$$\ddot{\theta}_A = -\frac{1}{\rho_b} |\mu_C^R J_A \gamma_C - \mu_A^R J_C \gamma_A| \dot{\theta}_A. \quad (14)$$

The equation implies that for general parameters θ_A is damped and does not rotate persistently along a given direction. However, if $\mu_C^R J_A \gamma_C \simeq \mu_A^R J_C \gamma_A$, the damping is weak and the two rotors persistently counter-rotate in a spontaneously chosen direction with the same speed and weak phase-locking interactions. We observe the three types of behavior in simulations as shown in the Supplementary Movies SM1–SM3 and Fig. 2b. On the contrary, it is easily seen that when both rotors are of the same type they always phase-lock, but do not exhibit persistent rotations. When both are type C (A) the rotors phase-lock with an angle difference 0 (π), see SM4 and SM5.

Formation of a traveling bound pair. — Here we again consider a type A and type C pair of semicircles. Numerical simulations show that, after a transient regime, the two bodies form a traveling bound pair with type A

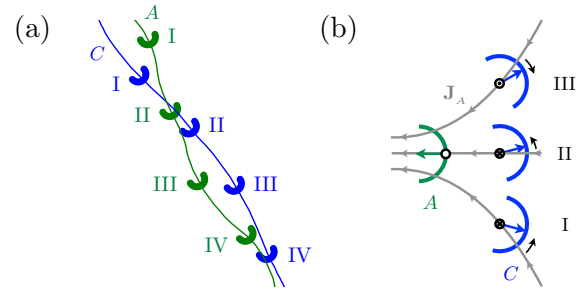


FIG. 3. (a) A stroboscopic image of a traveling bound pair obtained from the numerics, with consecutive positions marked by I–IV. All the parameters and units of the simulations are specified in Appendix A 4. (b) A schematic illustration of the torques experienced by a type C body in the current field of a type A body. I, II, and III indicate consecutive relative positions during the snake-like motion. Note that the torque directions are consistent with the resulting motion.

trailing type C (see Fig. 3a and movie SM6). This behavior can be qualitatively understood in the limit where $\mu_C^R \gg \mu_A^R$. Then the motion of type A is, to leading order, independent of type C while type C is strongly affected by type A . More precisely, the orientation of the type C body is dictated by its tendency to align γ_C with \mathbf{J}_A . This leads to a snake-like motion in front of the type A body explained graphically in Fig. 3b. Other pairings of semicircles lead to different phenomena including anti-alignment and the formation of bound pairs, although in this last case the effect depends on near-field interactions. These are expected to be less universal than the far-field interactions investigated here and we reserve their systematic study to future work.

In summary, we have explored the long-range interactions occurring generically between passive bodies placed in an active fluid. We have shown that, at first order in a multipole expansion, an asymmetric body generates dipolar currents which decay algebraically in space. These mediate generic long-range forces and torques between passive bodies which can be expressed in terms of a few single-body quantities. Interestingly, the interactions can be tuned by designing the shape of the bodies which may provide new routes for designing self-assembling materials. We gave two examples of dynamical phenomena induced by the far-field interactions. Considering also near-field effects should reveal many more. Finally, we note that the physics described is generic and relies only on the breaking of time reversal symmetry and a diffusive behavior at large length scale. Therefore, it should be present in a large class of active systems, with and without interactions.

Acknowledgments. — Y.B., N.N., and Y.K. are supported by an I-CORE Program of the Planning and Budgeting Committee of the Israel Science Foundation and an Israel Science Foundation grant. Y.B. is supported

in part at the Technion by a fellowship from the Lady Davis Foundation. A.P.S. is supported by the Gordon

and Betty Moor foundation through a PLS fellowship. X.X. is supported by Guangdong-Technion Postdoctoral Fellowship.

Appendix A: Simulation details

1. Active particles

Molecular dynamics simulations were performed employing an Euler time discretization scheme to integrate the two-dimensional overdamped Langevin dynamics in Eq. (1) of the main text. At each step of the simulation (from time t_i to $t_{i+1} = t_i + \Delta t$), the position and orientation of an active particle, given by (x, y, θ) , are updated by

$$\begin{aligned} x(t_{i+1}) &= x(t_i) + \Delta t \left[v \cos \theta(t_{i+1}) - \mu \partial_x V + \sqrt{2D_t/\Delta t} \eta_i^x \right], \\ y(t_{i+1}) &= y(t_i) + \Delta t \left[v \sin \theta(t_{i+1}) - \mu \partial_y V + \sqrt{2D_t/\Delta t} \eta_i^y \right], \\ \theta(t_{i+1}) &= \theta(t_i) + \Delta t \sqrt{2D_t/\Delta t} \xi_i, \end{aligned} \quad (\text{A1})$$

where v , μ , D_t , and $V = V(x, y)$ are defined in the main text, and $\eta_i^{x,y}$, ξ_i are i.i.d. random number sequences with a Gaussian distribution of zero mean and unit variance. The integration time step Δt is chosen to provide sufficient accuracy for a given set of parameters, with the highest value employed being $\Delta t = 10^{-2} \alpha^{-1}$. At each time step, we first update the orientation θ and then the spatial coordinates x and y . The tumbling dynamics are implemented by choosing a random time interval between tumbles from an exponential distribution with mean α^{-1} . If the next tumbling time τ falls between t_i and t_{i+1} , the interval is divided into two: a regular step takes place between t_i and τ , after which a new orientation $\theta(t_{i+1})$ and the next tumbling time are randomly chosen (the former from a uniform angular distribution). Finally the particle moves on with its new orientation from τ to t_{i+1} . For simulations of static bodies, the system is allowed to evolve for a sufficiently long time (adjusted according to the specific parameters in use) before any measurements take place, so that transient effects are removed.

2. Potentials of passive bodies

Passive bodies are described by localized potentials. The simplest body employed is a circular bead of radius R_b with a radial harmonic potential

$$V_b(\mathbf{r}) = \begin{cases} \frac{1}{2} \lambda (R_b - |\mathbf{r} - \mathbf{r}_0|)^2 & |\mathbf{r} - \mathbf{r}_0| < R_b, \\ 0 & |\mathbf{r} - \mathbf{r}_0| > R_b, \end{cases} \quad (\text{A2})$$

where $\mathbf{r}_0 = (x_0, y_0)$ is the center of the bead. The spring constant (or stiffness) λ determines the hard-core region, which extends from the center to a radius $R_b - \lambda^{-1}v/\mu$. Only the outer region of the disc surrounding this core can be penetrated by active particles. Due to the circular symmetry, the bead cannot produce any long-range density or current fields on its own.

We implemented passive bodies as rigid chains of the beads described above. For asymmetric bodies with nonzero

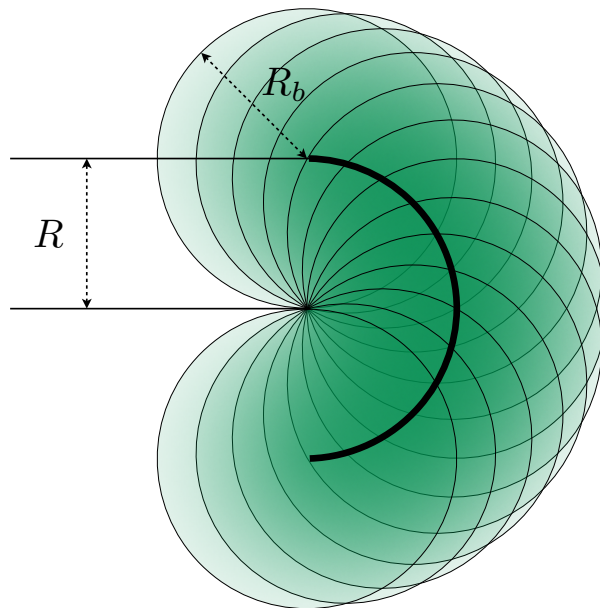


FIG. 4. An illustration of a semicircular body of radius R composed of 13 circular beads of the same radius $R_b = R$. The center of every bead lies on the arc of the semicircle (thick solid line), with any adjacent pair of them separated by equal angular distance.

dipole moment, we used semicircular bodies composed of identical beads. The beads are arranged so that their centers are placed on the arc of a semicircle of radius R . The centers of the two beads at the ends coincide with the tips of the semicircular arc, and all adjacent pairs of beads have equal angular distance from each other. The number of beads N is adjusted to create a sufficient overlap between neighbors, so that the arc of the semicircle is impenetrable to the active particles. A semicircle of radius R composed of $N = 13$ identical beads of the same radius $R_b = R$ is illustrated in Fig. 4.

In addition, we used rod-like bodies in Fig. 5 that have no dipole moment but non-vanishing quadrupole moment.

3. Dynamics of passive bodies

As stated in Eq. (12) of the main text, the overdamped dynamics of passive bodies are implemented by first calculating the forces and torques on each of them. At every time step, the total force and torque on body j are computed by

$$\begin{aligned} \mathbf{F}_j(t_i) &= \sum_k \nabla V_j(\mathbf{r}_k(t_i)) , \\ \boldsymbol{\tau}_j(t_i) &= \mathbf{e}_z \cdot \sum_k [\mathbf{r}_k(t_i) - \mathbf{R}_j(t_i)] \times \nabla V_j(\mathbf{r}_k(t_i)) , \end{aligned} \quad (\text{A3})$$

respectively, where \mathbf{r}_k denotes the position of the k -th active particle. The coordinates of body j are then updated as

$$\mathbf{R}_j(t_{i+1}) = \mathbf{R}_j(t_i) + \Delta t \mu_j^T \mathbf{F}_j(t_i), \quad (\text{A4})$$

$$\Theta_j(t_{i+1}) = \Theta_j(t_i) + \Delta t \mu_j^R \tau_j(t_i). \quad (\text{A5})$$

4. Simulation parameters

Here we describe the parameters used in simulations whose results are shown in the figures of the main text and the Supplementary Movies. In all simulations listed below, the active fluid is implemented by run-and-tumble particles with $v = \alpha = \mu = 1$ and $D_r = D_t = 0$. Time, lengths and forces are thus measured in units of α^{-1} , $l_r = v/\alpha$, and v/μ , respectively.

- In Fig. 1, body 1 is a semicircle of radius $R = l_r$, which is composed of 127 circular beads of radius $R_b = l_r/10$ and stiffness $\lambda = 20$. Its normalized dipole moment is measured to be $p_1/\rho_b \simeq 0.58$, headed from the convex side to the concave side of the semicircle. Body 2 is a circular bead of radius $l_r/6$ and stiffness $\lambda = 12$. Its normalized response coefficient (corresponding to \mathbb{R}_2 in the main text) is measured to be $R_2/\rho_b \simeq 0.54$. If body 2 is pinned at a point on the edge, γ_2 is a vector pointing at the center of the circle from the pinning point, whose magnitude is 0.091. The mean density of run-and-tumble particles is set to be $\rho_b = 1200$, and the system size is given by 70×70 with periodic boundaries.
- In Figs. 2, 3, and the Supplementary Movies, each semicircle has radius $R = l_r$ and is composed of 13 identical beads of radius $R_b = l_r$ and stiffness $\lambda = 2$. Type *C* semicircles rotate about the center of the semicircle, and type *A* semicircles rotate about the center of the middle bead. In Fig. 3, the translational mobilities of both semicircles are fixed at $\mu_C^T = \mu_A^T = 1$. The mean density of run-and-tumble particles is set to be $\rho_b = 800$, and the system size is given by 30×30 with periodic boundaries.

Appendix B: Derivation of far-field density and current

In this section, we present a detailed derivation of the far-field active particle density $\rho_j = \rho_j(\mathbf{r})$ created by a static body j , whose leading order behavior is given in Eqs. (4) and (5) of the main text. We start from the steady-state Fokker–Planck equation for the distribution $P_j = P_j(\mathbf{r}, \theta)$ of active particles

$$0 = -\nabla \cdot (v\mathbf{e}_\theta - \mu\nabla V_j - D_t\nabla) P_j - \alpha P_j + \frac{\alpha}{2\pi} \int d\theta P_j + D_r \partial_\theta^2 P_j, \quad (\text{B1})$$

which corresponds to the Langevin dynamics given by Eq. (1) of the main text. Next, we introduce the marginal distributions

$$\mathbf{m}_j^{(n)}(\mathbf{r}) \equiv \int d\theta P_j(\mathbf{r}, \theta) \begin{bmatrix} \cos(n\theta) \\ \sin(n\theta) \end{bmatrix} \quad (\text{B2})$$

for integers $n \geq 0$, with $\mathbf{m}_j^{(0)} = (\rho_j, 0)^T$. Multiplying both sides of Eq. (B1) by $\cos(n\theta)$ or $\sin(n\theta)$ and integrating over θ , we obtain the hierarchical relations

$$0 = -\nabla \cdot \left(v\mathbf{m}_j^{(1)} - \rho_j \mu \nabla V_j - D_t \nabla \rho_j \right), \quad (\text{B3})$$

$$0 = -(\alpha + D_r n^2)(1 - \mathbb{M}_j^{(n)})\mathbf{m}_j^{(n)} - \frac{v}{2} \left(\mathbb{D}\mathbf{m}_j^{(n-1)} - \mathbb{D}^\dagger \mathbf{m}_j^{(n+1)} \right), \quad (\text{B4})$$

where the second equation holds for integers $n \geq 1$, and we have defined the linear operators

$$\begin{aligned} \mathbb{M}_j^{(n)} &\equiv \frac{1}{\alpha + D_r n^2} [\mu \nabla \cdot (\nabla V_j) + D_t \nabla^2] \\ &= \frac{1}{\alpha + D_r n^2} [\mu (\nabla^2 V_j) + (\nabla V_j) \cdot \nabla + D_t \nabla^2], \end{aligned} \quad (\text{B5})$$

$$\mathbb{D} \equiv \begin{bmatrix} \partial_x & -\partial_y \\ \partial_y & \partial_x \end{bmatrix}, \quad \mathbb{D}^\dagger = \begin{bmatrix} -\partial_x & -\partial_y \\ \partial_y & -\partial_x \end{bmatrix}. \quad (\text{B6})$$

The operators \mathbb{D} and \mathbb{D}^\dagger form a conjugate pair satisfying

$$\mathbb{D}\mathbb{D}^\dagger = \mathbb{D}^\dagger\mathbb{D} = -\nabla^2. \quad (\text{B7})$$

We also note that solving Eq. (B4) for $\mathbf{m}_j^{(n)}$ gives

$$\begin{aligned} \mathbf{m}_j^{(n)} &= -\frac{v}{2(\alpha + D_r n^2)} \left(1 - \mathbb{M}_j^{(n)} \right)^{-1} \left(\mathbb{D}\mathbf{m}_j^{(n-1)} - \mathbb{D}^\dagger \mathbf{m}_j^{(n+1)} \right) \\ &= -\frac{v}{2(\alpha + D_r n^2)} \sum_{k=0}^{\infty} \left(\mathbb{M}_j^{(n)} \right)^k \left(\mathbb{D}\mathbf{m}_j^{(n-1)} - \mathbb{D}^\dagger \mathbf{m}_j^{(n+1)} \right), \end{aligned} \quad (\text{B8})$$

where the second equation is obtained by a formal expansion.

For $n = 1$ and $n = 2$, Eq. (B4) can be rewritten as

$$\mathbf{m}_j^{(1)} = \mathbb{M}_j^{(1)} \mathbf{m}_j^{(1)} - \frac{l_r}{2} \left(\nabla \rho_j + \mathbb{D}^\dagger \mathbf{m}_j^{(2)} \right), \quad (\text{B9})$$

$$\mathbf{m}_j^{(2)} = \mathbb{M}_j^{(2)} \mathbf{m}_j^{(2)} - \frac{l_r}{2} \frac{\alpha + D_r}{\alpha + 4D_r} \left(\mathbb{D}\mathbf{m}_j^{(1)} - \mathbb{D}^\dagger \mathbf{m}_j^{(3)} \right), \quad (\text{B10})$$

with $l_r \equiv v/(\alpha + D_r)$ representing the run length of each active particle. Applying $-v\nabla \cdot$ to both sides of Eq. (B9) and expressing $\mathbb{M}_j^{(1)}$ by Eq. (B5), we obtain

$$\begin{aligned} -\nabla \cdot \left(v\mathbf{m}_j^{(1)} \right) &= -\mu l_r \sum_{a,b} \partial_a \partial_b \left(\partial_a V_j \right) \left(\mathbf{m}_j^{(1)} \cdot \mathbf{e}_b \right) - D_t l_r \nabla^2 \nabla \cdot \mathbf{m}_j^{(1)} \\ &\quad + \frac{v l_r}{2} \left(\nabla^2 \rho_j + \nabla \cdot \mathbb{D}^\dagger \mathbf{m}_j^{(2)} \right), \end{aligned} \quad (\text{B11})$$

where the indices a and b run over the Cartesian coordinates $\{x, y\}$, and \mathbf{e}_b denotes the unit vector in the b -direction. This equation can be further expanded by replacing $\mathbf{m}_j^{(2)}$ with Eq. (B10), and then using Eq. (B5) with $n = 2$ and

Eq. (B7). One obtains

$$\begin{aligned}
-\nabla \cdot (v\mathbf{m}_j^{(1)}) &= \frac{vl_r}{2} \nabla^2 \rho_j - \mu l_r \sum_{a,b} \partial_a \partial_b (\partial_a V_j) (\mathbf{m}_j^{(1)} \cdot \mathbf{e}_b) \\
&\quad + \sum_{a,b,c} \partial_a \partial_b \partial_c (\mathbb{H}_j)_{abc} ,
\end{aligned} \tag{B12}$$

with a, b , and c running over $\{x, y\}$, and a rank-3 tensor \mathbb{H}_j satisfying

$$\begin{aligned}
\sum_{a,b,c} \partial_a \partial_b \partial_c (\mathbb{H}_j)_{abc} &= -D_t l_r \nabla^2 \nabla \cdot \mathbf{m}_j^{(1)} - \frac{vl_r^2}{4} \frac{\alpha + D_r}{\alpha + 4D_r} \left[\nabla^2 \nabla \cdot \mathbf{m}_j^{(1)} + \nabla \cdot (\mathbb{D}^\dagger)^2 \mathbf{m}_j^{(3)} \right] \\
&\quad + \frac{l_r^2}{2} \frac{\alpha + D_r}{\alpha + 4D_r} \nabla \cdot \mathbb{D}^\dagger \sum_a \partial_a [\mu (\partial_a V_j) + D_t \partial_a] \mathbf{m}_j^{(2)} .
\end{aligned} \tag{B13}$$

Using Eq. (B12) to replace $\mathbf{m}_j^{(1)}$ in Eq. (B3) leads to the two-dimensional Poisson equation

$$0 = D_{\text{eff}} \nabla^2 \rho_j + \mu \nabla \cdot (\rho_j \nabla V_j) - \mu l_r \sum_{a,b} \partial_a \partial_b (\partial_a V_j) (\mathbf{m}_j^{(1)} \cdot \mathbf{e}_b) + \sum_{a,b,c} \partial_a \partial_b \partial_c (\mathbb{H}_j)_{abc} , \tag{B14}$$

where $D_{\text{eff}} \equiv D_t + vl_r/2$ is the effective diffusion constant. We note that the equation is consistent with Eq. (2) of the main text, in which the rank-2 tensor \mathbb{G}_j is given by

$$(\mathbb{G}_j)_{ab} \equiv -\mu l_r (\partial_a V_j) (\mathbf{m}_j^{(1)} \cdot \mathbf{e}_b) + \sum_c \partial_c (\mathbb{H}_j)_{abc} . \tag{B15}$$

Applying the method of Green's functions, the solution to Eq. (B14) is obtained as

$$\begin{aligned}
\rho_j(\mathbf{r}) &= \rho_b - \frac{\beta_{\text{eff}}}{2\pi} \int d^2 \mathbf{r}' \ln |\mathbf{r} - \mathbf{r}'| \\
&\quad \times \left[\nabla' \cdot (\rho_j \nabla' V_j) - l_r \sum_{a,b} \partial'_a \partial'_b (\partial'_a V_j) (\mathbf{m}_j^{(1)} \cdot \mathbf{e}_b) + \frac{1}{\mu} \sum_{a,b,c} \partial'_a \partial'_b \partial'_c (\mathbb{H}_j)_{abc} \right] ,
\end{aligned} \tag{B16}$$

where $\beta_{\text{eff}} \equiv \mu/D_{\text{eff}}$ denotes the effective inverse temperature, and primed derivatives are with respect to \mathbf{r}' . In the far-field regime, i.e. when $r \equiv |\mathbf{r}|$ is greater than any other microscopic length scale, the integral in Eq. (B16) can be approximated by a multipole expansion

$$\rho_j(\mathbf{r}) \simeq \rho_b + \frac{\beta_{\text{eff}}}{2\pi} \left(\frac{\mathbf{r} \cdot \mathbf{p}_j}{r^2} + \frac{\mathbf{r} \cdot \mathbf{Q}_j \mathbf{r}}{2r^4} \right) . \tag{B17}$$

Here the dipole moment \mathbf{p}_j is given by

$$\mathbf{p}_j = - \int d^2 \mathbf{r}' \rho_j \nabla' V , \tag{B18}$$

and the quadrupole moment \mathbb{Q}_j satisfies

$$\begin{aligned}
(\mathbb{Q}_j)_{ab} = & -2 \int d^2 \mathbf{r}' \left\{ \rho_j (r'_a \partial'_b V_j + r'_b \partial'_a V_j) - l_r \left[(\partial'_a V_j) (\mathbf{m}_j^{(1)} \cdot \mathbf{e}_b) + (\partial'_b V_j) (\mathbf{m}_j^{(1)} \cdot \mathbf{e}_a) \right] \right. \\
& \left. - \delta_{ab} \left[\rho_j \mathbf{r}' \cdot \nabla' V_j - l_r (\nabla' V_j) \cdot \mathbf{m}_j^{(1)} \right] \right\}. \tag{B19}
\end{aligned}$$

Note that at dipole order there are no contributions from tensor \mathbb{G}_j defined in Eq. (B15), and that at quadrupole order there are no contributions from tensor \mathbb{H}_j expressed in Eq. (B13). In principle, one can calculate higher-order multipoles from the contributions of \mathbb{H}_j , which are beyond the scope of this work.

The results are consistent with Eqs. (3) and (4) of the main text. We also note that Eqs. (B18) and (B19) are *exact*; they do not rely on any further assumptions besides the far-field limit. Moreover, based on the equations, \mathbf{p}_j and \mathbb{Q}_j can be measured numerically using the marginal distributions ρ_j and $\mathbf{m}_j^{(1)}$ of active particles on body j . Both can also be estimated from the far-field behavior using Eq. (B17).

We now turn to the current density of active particles $\mathbf{J}_j = \mathbf{J}_j(\mathbf{r})$ generated by static body j . Since Eq. (B3) is a continuity equation $\nabla \cdot \mathbf{J}_j = 0$, the current density is given by

$$\mathbf{J}_j = v \mathbf{m}_j^{(1)} - \rho_j \mu \nabla V_j - D_t \nabla \rho_j = -D_{\text{eff}} \nabla \rho_j - \rho_j \mu \nabla V_j + v \mathbb{M}_j^{(1)} \mathbf{m}_j^{(1)} - \frac{v l_r}{2} \mathbb{D}^\dagger \mathbf{m}_j^{(2)}, \tag{B20}$$

where the second equation is obtained by replacing $\mathbf{m}_j^{(1)}$ with Eq. (B9). We now show that the last two terms in the equation are of order r^{-3} in the far-field. To see this, note that the recursive structure of Eq. (B8) implies $\mathbf{m}_j^{(n)} \sim \partial^n \rho_j + O(\partial^{n+2} \rho_j)$, with ∂ denoting a generic spatial derivative. In the far field we have $\mathbb{M}_j^{(1)} \sim \partial^2$ and $\mathbb{D}^\dagger \sim \partial$, thus we are left with

$$\begin{aligned}
\mathbf{J}_j(\mathbf{r}) = & -D_{\text{eff}} \nabla \rho_j + O(\partial^3 \rho_j) \\
\approx & -\frac{\mu}{2\pi} \left[\frac{\mathbf{p}_j}{r^2} - \frac{2(\mathbf{r} \cdot \mathbf{p}_j) \mathbf{r}}{r^4} \right] - \frac{\mu}{2\pi} \left[\frac{\mathbb{Q}_j \mathbf{r}}{r^4} - \frac{2(\mathbf{r} \cdot \mathbb{Q}_j \mathbf{r}) \mathbf{r}}{r^6} \right], \tag{B21}
\end{aligned}$$

which is dominated by the diffusive component. The dipole component of this expression is given in Eq. (5) of the main text. Moreover, by integrating both sides of Eq. (B20) over the entire space, we obtain

$$\int d^2 \mathbf{r} \mathbf{J}_j = -\mu \int d^2 \mathbf{r} \rho_j \nabla V_j = \mu \mathbf{p}_j, \tag{B22}$$

which is an exact relation for this class of model, derived for more general cases in [25].

Appendix C: Interactions between distant bodies

1. Far-field forces and torques

We consider a pair of static bodies in an active fluid of bulk density ρ_b . Their interactions with active particles are described by potentials V_1 and V_2 . Body 2 is positioned at the origin ($\mathbf{R}_2 = 0$), and body 1 is at a distant location

$\mathbf{R}_1 = \mathbf{r}_{12}$. Extending Eq. (B16) to the two-body case, the marginal distributions $\rho = \rho(\mathbf{r})$ and $\mathbf{m}^{(n)} = \mathbf{m}^{(n)}(\mathbf{r})$ of the active particles satisfy

$$\begin{aligned} \rho(\mathbf{r}) &= \rho_b - \frac{\beta_{\text{eff}}}{2\pi} \int d^2\mathbf{r}' \ln |\mathbf{r} - \mathbf{r}'| \\ &\times \left[\nabla' \cdot (\rho \nabla' V) - l_r \sum_{a,b} \partial'_a \partial'_b (\partial'_a V) (\mathbf{m}^{(1)} \cdot \mathbf{e}_b) + \frac{1}{\mu} \sum_{a,b,c} \partial'_a \partial'_b \partial'_c (\mathbb{H})_{abc} \right], \end{aligned} \quad (\text{C1})$$

where $V = V_1 + V_2$ and \mathbb{H} are defined as in Eq. (B13) but with the index j dropped, so that they correspond to the full two-body problem. In order to obtain the force \mathbf{F}_{12} applied by body 1 on body 2, we focus on \mathbf{r} in the vicinity of body 2. To this end, we divide the spatial integral into two domains: Ω_1 covers the domain of body 1, and Ω_1^c covers the rest of the space. Then the integral can be decomposed as

$$\begin{aligned} \rho(\mathbf{r}) &= \rho_b - \frac{\beta_{\text{eff}}}{2\pi} \int_{\Omega_1} d^2\mathbf{r}' \ln |\mathbf{r} - \mathbf{r}'| \\ &\times \left[\nabla' \cdot (\rho \nabla' V_1) - l_r \sum_{a,b} \partial'_a \partial'_b (\partial'_a V_1) (\mathbf{m}^{(1)} \cdot \mathbf{e}_b) + \frac{1}{\mu} \sum_{a,b,c} \partial'_a \partial'_b \partial'_c (\mathbb{H})_{abc} \right] \\ &- \frac{\beta_{\text{eff}}}{2\pi} \int_{\Omega_1^c} d^2\mathbf{r}' \ln |\mathbf{r} - \mathbf{r}'| \\ &\times \left[\nabla' \cdot (\rho \nabla' V_2) - l_r \sum_{a,b} \partial'_a \partial'_b (\partial'_a V_2) (\mathbf{m}^{(1)} \cdot \mathbf{e}_b) + \frac{1}{\mu} \sum_{a,b,c} \partial'_a \partial'_b \partial'_c (\mathbb{H})_{abc} \right], \end{aligned} \quad (\text{C2})$$

For large r_{12} , the contribution from Ω_1 can be expressed by a multipole expansion

$$\begin{aligned} \rho(\mathbf{r}) &= \rho_b - \frac{\beta_{\text{eff}}}{2\pi} \int_{\Omega_1^c} d^2\mathbf{r}' \ln |\mathbf{r} - \mathbf{r}'| \\ &\times \left[\nabla' \cdot (\rho \nabla' V_2) - l_r \sum_{a,b} \partial'_a \partial'_b (\partial'_a V_2) (\mathbf{m}^{(1)} \cdot \mathbf{e}_b) + \frac{1}{\mu} \sum_{a,b,c} \partial'_a \partial'_b \partial'_c (\mathbb{H})_{abc} \right] \\ &+ \frac{\beta_{\text{eff}}}{2\pi} \left[\frac{\mathbf{r}_{12} \cdot \tilde{\mathbf{p}}_1}{r_{12}^2} + \frac{\mathbf{r} \cdot \tilde{\mathbf{p}}_1}{r_{12}^2} - \frac{2(\mathbf{r} \cdot \mathbf{r}_{12})(\mathbf{r}_{12} \cdot \tilde{\mathbf{p}}_1)}{r_{12}^4} + \frac{\mathbf{r}_{12} \cdot \tilde{\mathbf{Q}}_1 \mathbf{r}_{12}}{2r_{12}^4} \right] + O(r_{12}^{-3}), \end{aligned} \quad (\text{C3})$$

where $\tilde{\mathbf{p}}_j$ and $\tilde{\mathbf{Q}}_j$ are the dipole and quadrupole moments of body j , respectively, given by

$$\tilde{\mathbf{p}}_j = - \int d^2\mathbf{r}' \rho \nabla' V_j, \quad (\text{C4})$$

$$\begin{aligned} (\tilde{\mathbf{Q}}_j)_{ab} &= -2 \int d^2\mathbf{r}' \left\{ \rho (r'_a \partial'_b V_j + r'_b \partial'_a V_j) - l_r \left[(\partial'_a V_j) (\mathbf{m}^{(1)} \cdot \mathbf{e}_b) + (\partial'_b V_j) (\mathbf{m}^{(1)} \cdot \mathbf{e}_a) \right] \right. \\ &\left. - \delta_{ab} \left[\rho \mathbf{r}' \cdot \nabla' V_j - l_r (\nabla' V_j) \cdot \mathbf{m}^{(1)} \right] \right\}, \end{aligned} \quad (\text{C5})$$

which also takes into account the influence of the other body through ρ and $\mathbf{m}^{(1)}$. We can further simplify the integral in Eq. (C3) by noting that, even if we add Ω_1 to the range of the integral, the contribution of the added domain is of order r_{12}^{-3} due to vanishing V_2 and the three spatial derivatives in front of \mathbb{H} . Thus, up to order r_{12}^{-2} , the integral over

Ω_1^c can be safely replaced with the one over the entire space

$$\begin{aligned} \rho(\mathbf{r}) = & \rho_b - \frac{\beta_{\text{eff}}}{2\pi} \int d^2\mathbf{r}' \ln|\mathbf{r} - \mathbf{r}'| \left[\nabla' \cdot (\rho \nabla' V_2) - l_r \sum_{a,b} \partial'_a \partial'_b (\partial'_a V_2) (\mathbf{m}^{(1)} \cdot \mathbf{e}_b) \right] \\ & + \frac{\beta_{\text{eff}}}{2\pi} \left[\frac{\mathbf{r}_{12} \cdot \tilde{\mathbf{p}}_1}{r_{12}^2} + \frac{\mathbf{r} \cdot \tilde{\mathbf{p}}_1}{r_{12}^2} - \frac{2(\mathbf{r} \cdot \mathbf{r}_{12})(\mathbf{r}_{12} \cdot \tilde{\mathbf{p}}_1)}{r_{12}^4} + \frac{\mathbf{r}_{12} \cdot \tilde{\mathbf{Q}}_1 \mathbf{r}_{12}}{2r_{12}^4} \right] + O(r_{12}^{-3}) . \end{aligned} \quad (\text{C6})$$

Next, treating r_{12} as a large parameter, Eq. (C6) can be solved using the perturbative series

$$\rho(\mathbf{r}) = \sum_{n=0}^{\infty} \frac{1}{r_{12}^n} \rho^{(n)}(\mathbf{r}) , \quad \mathbf{m}^{(1)} = \sum_{n=0}^{\infty} \frac{1}{r_{12}^n} \mathbf{m}^{(1,n)}(\mathbf{r}) . \quad (\text{C7})$$

At zeroth order, Eq. (C6) is indistinguishable from Eq. (B16) with $j = 2$, which reflects that at this order the presence of body 1 does not affect the density profile in the vicinity of body 2. Thus $\rho^{(0)} = \rho_2$ and $\mathbf{m}^{(1,0)} = \mathbf{m}_2^{(1)}$, where ρ_2 and $\mathbf{m}_2^{(1)}$ are the marginal distributions of active particles created by an isolated body 2.

Proceeding to the next order, we obtain

$$\begin{aligned} \rho^{(1)}(\mathbf{r}) = & -\frac{\beta_{\text{eff}}}{2\pi} \int d^2\mathbf{r}' \ln|\mathbf{r} - \mathbf{r}'| \left[\nabla' \cdot (\rho^{(1)} \nabla' V_2) - l_r \sum_{a,b} \partial'_a \partial'_b (\partial'_a V_2) (\mathbf{m}^{(1,1)} \cdot \mathbf{e}_b) \right] \\ & + \frac{\beta_{\text{eff}}}{2\pi} \frac{\mathbf{r}_{12} \cdot \tilde{\mathbf{p}}_1}{r_{12}} . \end{aligned} \quad (\text{C8})$$

At this order $\tilde{\mathbf{p}}_1$ can be replaced with \mathbf{p}_1 , the dipole moment of the isolated body 1 given by Eq. (B18). We note that Eqs. (B16) and (C8) have the same form, the only difference being that the constant ρ_b in the former is changed to the dipole contribution $\frac{\beta_{\text{eff}}}{2\pi} \frac{\mathbf{r}_{12} \cdot \mathbf{p}_1}{r_{12}}$ in the latter. Due to the linearity of these equations, the solution to Eq. (C8) is simply

$$\rho^{(1)}(\mathbf{r}) = \frac{\beta_{\text{eff}}}{2\pi\rho_b} \frac{\mathbf{r}_{12} \cdot \mathbf{p}_1}{r_{12}} \rho_2(\mathbf{r}) , \quad \mathbf{m}^{(1,1)}(\mathbf{r}) = \frac{\beta_{\text{eff}}}{2\pi\rho_b} \frac{\mathbf{r}_{12} \cdot \mathbf{p}_1}{r_{12}} \mathbf{m}_2^{(1)}(\mathbf{r}) . \quad (\text{C9})$$

Thus the leading-order force exerted by body 1 on body 2 is

$$\mathbf{F}_{12}^{(1)} \equiv \frac{1}{r_{12}} \int d^2\mathbf{r} \rho^{(1)}(\mathbf{r}) \nabla V_2 = -\frac{\beta_{\text{eff}}}{2\pi\rho_b} \frac{\mathbf{r}_{12} \cdot \mathbf{p}_1}{r_{12}^2} \mathbf{p}_2 , \quad (\text{C10})$$

which gives $\mathbf{F}_{12}^{\text{non-sym}}$ shown in Eq. (6) of the main text. According to Eq. (C4), this force also gives the leading-order correction to the dipole moment of body 2, so that

$$\tilde{\mathbf{p}}_2 = \mathbf{p}_2 - \mathbf{F}_{12}^{(1)} + O(r_{12}^{-2}) = \mathbf{p}_2 + \frac{\beta_{\text{eff}}}{2\pi\rho_b} \frac{\mathbf{r}_{12} \cdot \mathbf{p}_1}{r_{12}^2} \mathbf{p}_2 + O(r_{12}^{-2}) . \quad (\text{C11})$$

Similarly, the leading-order torque exerted by body 1 on body 2 satisfies

$$\boldsymbol{\tau}_{12}^{(1)} \equiv \frac{1}{r_{12}} \int d^2\mathbf{r} \rho^{(1)}(\mathbf{r}) \mathbf{r} \times \nabla V_2 = \frac{\beta_{\text{eff}}}{2\pi\rho_b} \frac{\mathbf{r}_{12} \cdot \mathbf{p}_1}{r_{12}^2} \boldsymbol{\tau}_2 , \quad (\text{C12})$$

where $\boldsymbol{\tau}_2 \equiv \int d^2\mathbf{r} \rho_2 \mathbf{r} \times \nabla V_2$ is the self-torque of the isolated body 2, as defined in the main text. This gives $\boldsymbol{\tau}_{12}^{\text{non-sym}}$ in Eq. (9) of the main text.

The equation for the next order is obtained by using Eq. (C6) and expanding $\tilde{\mathbf{p}}_1$ to order r_{12}^{-1} using Eq. (C11), with the body indices 1 and 2 exchanged. This gives

$$\begin{aligned} \rho^{(2)}(\mathbf{r}) = & -\frac{\beta_{\text{eff}}}{2\pi} \int_2 d^2\mathbf{r}' \ln |\mathbf{r} - \mathbf{r}'| \left[\nabla' \cdot (\rho^{(2)} \nabla' V_2) - l_r \sum_{a,b} \partial'_a \partial'_b (\partial'_a V_2) (\mathbf{m}^{(1,2)} \cdot \mathbf{e}_b) \right] \\ & + \rho_b^{(2)} - \frac{1}{D_{\text{eff}}} \mathbf{r} \cdot \mathbf{J}_b^{(2)}, \end{aligned} \quad (\text{C13})$$

where we introduced the effective bulk density

$$\rho_b^{(2)} \equiv \frac{\beta_{\text{eff}}}{2\pi} \left[\frac{\beta_{\text{eff}}(\mathbf{r}_{12} \cdot \mathbf{p}_2)(\mathbf{p}_1 \cdot \mathbf{r}_{12})}{2\pi \rho_b r_{12}^2} + \frac{\mathbf{r}_{12} \cdot \mathbb{Q}_1 \mathbf{r}_{12}}{2r_{12}^2} \right], \quad (\text{C14})$$

which is created by the induced dipole and the quadrupole moments of body 1, and the effective bulk current

$$\mathbf{J}_b^{(2)} \equiv -\frac{\mu}{2\pi} \left[\mathbf{p}_1 - \frac{2(\mathbf{r}_{12} \cdot \mathbf{p}_1) \mathbf{r}_{12}}{r_{12}^2} \right] = r_{12}^2 \mathbf{J}_1^{(2)}(\mathbf{r}_{12}), \quad (\text{C15})$$

with

$$\mathbf{J}_j^{(2)}(\mathbf{r}_{12}) \equiv -\frac{\mu}{2\pi} \left[\frac{\mathbf{p}_j}{r_{12}^2} - \frac{2(\mathbf{r}_{12} \cdot \mathbf{p}_j) \mathbf{r}}{r_{12}^4} \right] \quad (\text{C16})$$

denoting the dipole current generated by body j given in Eq. (B21). One observes that Eq. (C13) is almost similar in structure to Eq. (B16) except for the last term, which imposes a boundary condition

$$-D_{\text{eff}} \lim_{r \rightarrow \infty} \nabla \rho^{(2)} = \mathbf{J}_b^{(2)}. \quad (\text{C17})$$

Thus $\rho^{(2)}$ and $\mathbf{m}^{(1,2)}$ in Eq. (C13) can be interpreted as the marginal distributions of active particles observed in a reference frame comoving with body 2 at a constant velocity

$$\mathbf{u} \equiv -\frac{\mathbf{J}_b^{(2)}}{\rho_b^{(2)}} = \frac{2D_{\text{eff}} \rho_b [r_{12}^2 \mathbf{p}_1 - 2(\mathbf{r}_{12} \cdot \mathbf{p}_1) \mathbf{r}_{12}]}{\beta_{\text{eff}}(\mathbf{r}_{12} \cdot \mathbf{p}_2)(\mathbf{p}_1 \cdot \mathbf{r}_{12}) + \pi \rho_b \mathbf{r}_{12} \cdot \mathbb{Q}_1 \mathbf{r}_{12}}, \quad (\text{C18})$$

with the bulk density of the active fluid given by $\rho_b^{(2)}$.

The above result implies that at this order the force acting on body 2 is identical to the steady-state force on it when the body is dragged at constant velocity \mathbf{u} through an active fluid of bulk density $\rho_b^{(2)}$. Denoting this force by $\mathbf{F}_2^{(2)}(\mathbf{u})$ and using the fact that the particles are noninteracting, we can write

$$\mathbf{F}_{12}^{(2)} \equiv \frac{1}{r_{12}^2} \int_2 d^2\mathbf{r} \rho^{(2)}(\mathbf{r}) \nabla V_2 = \mathbf{F}_2^{(2)}(\mathbf{u}) = \frac{1}{r_{12}^2} \frac{\rho_b^{(2)}}{\rho_b} \mathbf{F}_2^{(0)}(\mathbf{u}), \quad (\text{C19})$$

with $\mathbf{F}_2^{(0)}(\mathbf{u})$ being the steady-state force experienced by body 2 dragged at velocity \mathbf{u} through an active fluid of

density ρ_b . When \mathbf{u} is sufficiently small (see the discussion in Sec. C2), we may use a linear approximation

$$\mathbf{F}_{12}^{(2)} \simeq \frac{1}{r_{12}^2} \left(\frac{\rho_b^{(2)}}{\rho_b} \mathbf{p}_2 - \frac{\rho_b^{(2)}}{\rho_b} \mathbb{R}_2 \mathbf{u} \right) = \frac{1}{r_{12}^2} \frac{\rho_b^{(2)}}{\rho_b} \mathbf{p}_2 + \frac{1}{\rho_b} \mathbb{R}_2 \mathbf{J}_1^{(2)}(\mathbf{r}_{12}), \quad (\text{C20})$$

where \mathbb{R}_2 is a response matrix describing the drag force exerted by an active fluid of bulk density ρ_b . Note that the second term of the rhs corresponds to the leading-order term of $\mathbf{F}_{12}^{\text{sym}}$ shown in Eq. (7) of the main text. Similarly, at this order the torque applied by body 1 on body 2 is obtained as

$$\boldsymbol{\tau}_{12}^{(2)} = \frac{1}{r_{12}^2} \frac{\rho_b^{(2)}}{\rho_b} \boldsymbol{\tau}_2(\mathbf{u}), \quad (\text{C21})$$

where $\boldsymbol{\tau}_2(\mathbf{u})$ is the torque felt by body 2 moving at a constant velocity \mathbf{u} in an active fluid of bulk density ρ_b . When $\mathbf{u} = (u_x, u_y)^T$ is sufficiently small, we may use a linear approximation

$$\boldsymbol{\tau}_{12}^{(2)} \simeq \frac{1}{r_{12}^2} \left[\frac{\rho_b^{(2)}}{\rho_b} \boldsymbol{\tau}_2^{(0)} + \frac{\rho_b^{(2)}}{\rho_b} \left(u_x \frac{\partial}{\partial u_x} \boldsymbol{\tau}_2(\mathbf{u}) \cdot \mathbf{e}_z + u_y \frac{\partial}{\partial u_y} \boldsymbol{\tau}_2(\mathbf{u}) \cdot \mathbf{e}_z \right) \mathbf{e}_z \right] \Bigg|_{\mathbf{u}=0}. \quad (\text{C22})$$

Defining the vector

$$\boldsymbol{\gamma}_2 \equiv \left[\begin{array}{c} -\frac{\partial}{\partial u_y} \boldsymbol{\tau}_2(\mathbf{u}) \cdot \mathbf{e}_z \\ \frac{\partial}{\partial u_x} \boldsymbol{\tau}_2(\mathbf{u}) \cdot \mathbf{e}_z \end{array} \right] \Bigg|_{\mathbf{u}=0} = - [\nabla_{\mathbf{u}} \times \boldsymbol{\tau}_2(\mathbf{u})] \Big|_{\mathbf{u}=0}, \quad (\text{C23})$$

which is also shown in Eq. (10) of the main text, we can write

$$\boldsymbol{\tau}_{12}^{(2)} \simeq \frac{1}{r_{12}^2} \left(\frac{\rho_b^{(2)}}{\rho_b} \boldsymbol{\tau}_2^{(0)} - \frac{\rho_b^{(2)}}{\rho_b} \boldsymbol{\gamma}_2 \times \mathbf{u} \right) = \frac{1}{r_{12}^2} \frac{\rho_b^{(2)}}{\rho_b} \boldsymbol{\tau}_2^{(0)} + \frac{1}{\rho_b} \boldsymbol{\gamma}_2 \times \mathbf{J}_1^{(2)}(\mathbf{r}_{12}), \quad (\text{C24})$$

whose second term on the rhs corresponds to $\boldsymbol{\tau}_{12}^{\text{sym}}$ in Eq. (10) of the main text.

Repeating similar procedures, we can obtain interactions which are higher-order in r_{12}^{-1} . These are important for bodies whose leading-order interactions stem from higher-order multipoles. For instance, when bodies 1 and 2 are both rod-like, all interactions at the orders discussed above are zero. The leading-order interaction between the two rods is expected to be controlled by quadrupole moments, which appear at the next order in the perturbative treatment, decaying as r_{12}^{-3} . This is numerically checked for the force in Fig. 5 for a pair of rod-like bodies immersed in an active fluid of run-and-tumble particles. While numerical limitations prohibit us from verifying the result unambiguously, we find the numerics consistent with our prediction.

2. Limit of small u

In the following we elaborate on the meaning of linear approximations for small $u \equiv |\mathbf{u}|$ used in Eqs. (C20) and (C24). Such approximations are justified when the change of the density $\Delta\rho$ induced by \mathbf{u} is much smaller than the original density in the vicinity of the isolated body 2. We note that \mathbf{u} introduces a global force $-\mathbf{u}/\mu$, which acts on each active particle. When this force is much weaker than the average force felt by each active particle at $\mathbf{u} = 0$,

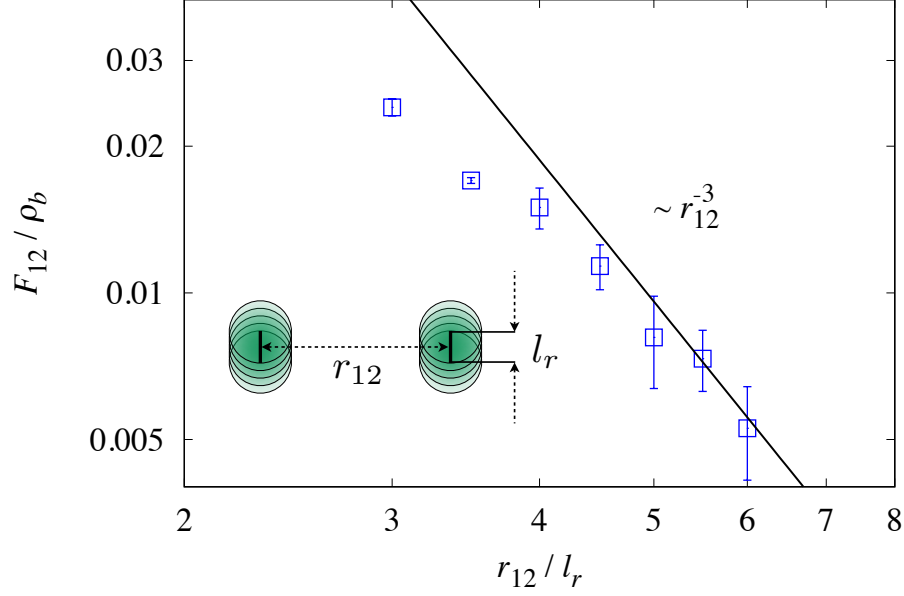


FIG. 5. The magnitude of the force $F_{12} \equiv |\mathbf{F}_{12}|$, normalized by the bulk density ρ_b of the ambient active fluid, between a pair of rod-like bodies, which are parallel and separated by a normalized distance r_{12}/l_r , where l_r is the run length of active particles. Each body consists of 5 identical beads of radius $R_b = l_r$ and stiffness $\lambda = 2$, whose centers are aligned at equal distances from each other along a straight segment of length l_r . The active fluid is implemented by run-and-tumble particles of bulk density $\rho_b = 4800$ in a system of size 30×30 (see Sec. A 4 for the other parameters and the units used). The simulation results (symbols) are consistent with a scaling behavior $F_{12} \sim r_{12}^{-3}$.

$\Delta\rho$ induced by the former can be treated as a small quantity. The scale of the force per unit length exerted by the active particles on the body is given by $P \equiv \rho_b/\beta_{\text{eff}}$, which is the pressure applied by the active particles on a flat wall [33–35, 41]. Denoting by d_2 the penetration depth of body 2, the number of active particles per unit length interacting with body 2 is proportional to $\rho_b d_2$. Thus, taking $\beta_{\text{eff}} \sim \mu/D_{\text{eff}} \sim \mu/(v l_r)$ (which holds for small D_t), the average force on each active particle is given by

$$\frac{P}{\rho_b d_2} \sim \frac{v l_r}{\mu d_2}. \quad (\text{C25})$$

Comparing this with u/μ , the small u limit can be translated into the condition

$$d_2 \ll \frac{v l_r}{u}. \quad (\text{C26})$$

To check when this condition is met in our problem of two interacting bodies, we use Eq. (C18). It shows that u has the scaling behavior

$$u \sim \min \left[\frac{D_{\text{eff}}^2 \rho_b}{\mu p_2}, \frac{D_{\text{eff}} p_1}{|\mathcal{Q}_1|} \right], \quad (\text{C27})$$

where $p_j = |\mathbf{p}_j|$. The first term on the rhs satisfies

$$\frac{D_{\text{eff}}^2 \rho_b}{\mu p_2} \sim \frac{\rho_b v l_r}{\beta_{\text{eff}} p_2} \sim \frac{P l_r}{p_2} v. \quad (\text{C28})$$

Thus, using $l_r = D_{\text{eff}}/v$ in Eqs. (C27) and (C26), one obtains the condition for small u as

$$d_2 \ll \max \left[\frac{p_2}{P}, \frac{|Q_1|}{p_1} \right]. \quad (\text{C29})$$

The physical interpretation of this condition is as follows. When $P d_2 \ll p_2$, the force \mathbf{p}_2 generated from the ratchet-like effect of body 2 is much larger than the scale $P d_2$ supported by the bulk active fluid. In this case, the far-field effects of body 1 are much smaller than the changes created by body 2 on itself. On the other hand, the second term implies that the effects of the dipole current generated by body 1 on the density near body 2 is much smaller than those of the quadrupole corrections. This condition is clearly only relevant for bodies with a very small dipole moment. When either of these two conditions is met, the influence of the dipole current made by body 1 can be described by a linear approximation.

Appendix D: Adiabatic limit

Here we elaborate on the adiabatic limit assumed for analyzing the dynamics of moving bodies. Consider first the case of an isolated body moving in an active fluid. As shown above, the active particles outside the body (where $V_j = 0$) behave as a diffusive fluid characterized by an effective diffusivity D_{eff} . Therefore, a density modulation, caused by the moving body, will spread the distance of the body l_j on a time scale t_s set by $l_j \sim \sqrt{D_{\text{eff}} t_s}$. For the adiabatic approximation to hold, this process has to be fast enough so that the density near the body will be well approximated by that obtained from a non-moving body. Namely, we require that on this time scale the body should move a distance much smaller than its size, or $v_j t_s \ll l_j$. Here v_j is the velocity of the body. This gives the condition for the validity of the approximation for a single moving body as

$$v_j \ll \frac{D_{\text{eff}}}{l_j}. \quad (\text{D1})$$

It is straightforward to extend these considerations for two interacting bodies i and j . One finds that the condition is then given by

$$\max\{v_i, v_j\} \ll \frac{D_{\text{eff}}}{r_{ij}}, \quad (\text{D2})$$

where r_{ij} is the distance between the bodies. We note that, despite these rather strict conditions, our results give much predictive power when used in numerics which do not obey these criteria.

Appendix E: Perturbative solutions for multipole moments

In this section we present perturbative solutions in the strength of the potential for the dipole and quadrupole moments of body j , assuming that changes in density occur on scales larger than the run length l_r . For simplicity, we focus on the case when the translational degrees of freedom are unaffected by the Gaussian white noise ($D_t = 0$). The generalization to the cases with $D_t \neq 0$ is straightforward but tedious.

To this end, we revisit Eq. (B14) for the steady-state density profile ρ_j . Using Eq. (B8) iteratively, $\mathbf{m}_j^{(1)}$ and $\mathbf{m}_j^{(2)}$ can be expressed in terms of ρ_j and $\mathbf{m}_j^{(3)}$. Then we divide both sides of Eq. (B14) by D_{eff} to obtain

$$\begin{aligned} \nabla^2 \rho_j = & -\beta_{\text{eff}} \nabla \cdot (\rho_j \nabla V_j) - \frac{\beta_{\text{eff}} l_r^2}{2} \sum_{a,b} \partial_a \partial_b (\partial_a V_j) (\partial_b \rho_j) \\ & + \frac{\beta_{\text{eff}} l_r^2}{4} \frac{\alpha + D_r}{\alpha + 4D_r} \nabla^2 \nabla \cdot (\rho_j \nabla V_j) + O(l_r^3 \partial^3). \end{aligned} \quad (\text{E1})$$

Here $O(l_r^3 \partial^3)$ indicates a third or higher-order spatial derivative, with each derivative multiplied by l_r . Terms of this order can be identified by noting that, according to Eq. (B8), reducing $\mathbf{m}_j^{(n)}$ to $\mathbf{m}_j^{(n-1)}$ always involves a factor of l_r , and that the operator $\mathbb{M}_j^{(1)}$ defined in Eq. (B5) can be rewritten as

$$\mathbb{M}_j^{(1)} = \frac{\mu}{\alpha + D_r} \nabla \cdot \nabla V_j = \frac{\beta_{\text{eff}} l_r^2}{2} \nabla \cdot \nabla V_j. \quad (\text{E2})$$

When l_r is much shorter than the length scale over which the density distribution changes (e.g. the penetration depth d_j), each $l_r \partial$ yields a small factor l_r/d_j . Thus $O(l_r^3 \partial^3)$ is negligible compared to terms of the order $l_r^2 \partial^2$. With this in mind, under the assumption of the weak potential ($\beta_{\text{eff}} V_j \ll 1$), we can solve Eq. (E1) by a perturbation series $\rho_j = \sum_{k=0}^{\infty} \rho_{j,k}$ with $\rho_{j,k} \sim (\beta_{\text{eff}} V)^k$.

At zeroth order, the system is unaffected by the presence of body j . Therefore $\rho_{j,0}$ is simply given by the bulk density ρ_b , which is constant over the entire space.

The next order can be obtained iteratively by Eq. (E1), which gives

$$\nabla^2 \rho_{j,1} = -\rho_b \beta_{\text{eff}} \nabla^2 V_j + \frac{\rho_b \beta_{\text{eff}} l_r^2}{4} \frac{\alpha + D_r}{\alpha + 4D_r} (\nabla^2)^2 V_j + O(l_r^3 \partial^3), \quad (\text{E3})$$

whose solution is

$$\rho_{j,1}(\mathbf{r}) = -\rho_b \beta_{\text{eff}} V_j + \frac{\rho_b \beta_{\text{eff}} l_r^2}{4} \frac{\alpha + D_r}{\alpha + 4D_r} \nabla^2 V_j + O\left(\frac{l_r^3}{d_j^3}\right). \quad (\text{E4})$$

Using this relation in Eq. (B18) yields a zero dipole moment, implying $\mathbf{p}_j = O(\beta_{\text{eff}}^2 V_j^2, l_r^3/d_j^3)$. On the other hand, combining Eq. (E4) with Eq. (B19) and using the relations

$$\begin{aligned} \int d^2 \mathbf{r}' (\nabla'^2 V_j) r'_a \partial'_b V_j &= - \int d^2 \mathbf{r}' \left[(\partial'_a V_j) (\partial'_b V_j) - \frac{\delta_{ab}}{2} (\nabla' V_j)^2 \right], \\ \int d^2 \mathbf{r}' V_j r'_a \partial'_b V_j &= - \frac{\delta_{ab}}{2} \int d^2 \mathbf{r}' V_j^2, \end{aligned} \quad (\text{E5})$$

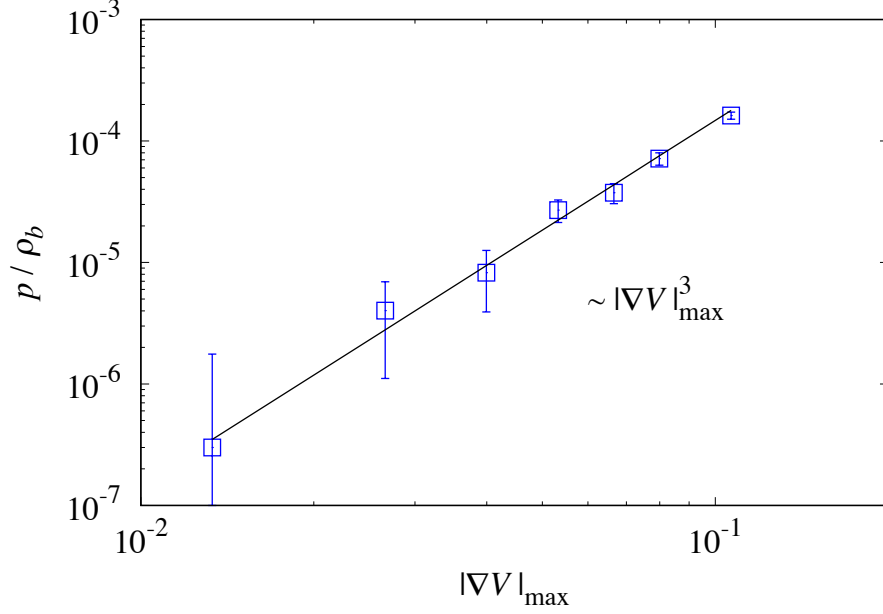


FIG. 6. The dipole moment p , normalized by the bulk density ρ_b of the ambient active fluid, of an asymmetric body as a function of the maximal force $|\nabla V|_{\max}$ applied by its potential. The potential is a skewed Schwartz bell, which is $V(r, \theta) = \lambda e^{-1/(1-r^2)} (1 + r \cos \theta)$ for $r \leq 1$ and zero for $r \geq 1$. The dipole moment lies along the x -axis, the only asymmetric direction of the potential. The active fluid consists of noninteracting run-and-tumble particles with $v = \mu = 1$, $\alpha = 0.3$, and $\rho_b = 3.75$ in a system of size 40×40 (in arbitrary units). The simulation results (symbols) are compared with the prediction (solid line) of Eq. (E13).

one finds the quadrupole moment

$$(\mathbb{Q}_j)_{ab} = -\rho_b \beta_{\text{eff}}^2 l_r^2 \frac{\alpha + 7D_r}{\alpha + 4D_r} \int d^2 \mathbf{r} \left[(\partial_a V_j)(\partial_b V_j) - \frac{\delta_{ab}}{2} (\nabla V_j)^2 \right] + O\left(\beta_{\text{eff}}^2 V_j^2, \frac{l_r^3}{d_j^3}\right). \quad (\text{E6})$$

Thus, if $|\nabla V_j|_{\max}$ denotes the maximal force applied by the potential of body j , the quadrupole moment satisfies

$$|\mathbb{Q}_j| \sim l_r^2 |\nabla V_j|_{\max}^2 \quad (\text{E7})$$

in the limit of weak potential and small run length.

To obtain the leading dipole moment, we proceed to the next order. From Eqs. (E1) and (E4), one obtains

$$\begin{aligned} \nabla^2 \rho_{j,2} &= \frac{\rho_b \beta_{\text{eff}}^2}{2} \nabla^2 V_j^2 - \frac{\rho_b \beta_{\text{eff}}^2 l_r^2}{8} \frac{\alpha + D_r}{\alpha + 4D_r} (\nabla^2)^2 V_j^2 - \frac{\rho_b \beta_{\text{eff}}^2 l_r^2}{4} \frac{\alpha + D_r}{\alpha + 4D_r} \nabla \cdot (\nabla V_j) \nabla^2 V_j \\ &\quad + \frac{\rho_b \beta_{\text{eff}}^2 l_r^2}{2} \sum_{a,b} \partial_a \partial_b (\partial_a V_j)(\partial_b V_j) + O(l_r^3 \partial^3). \end{aligned} \quad (\text{E8})$$

Noting

$$\begin{aligned}
\int d^2\mathbf{r}' \ln|\mathbf{r}-\mathbf{r}'| \nabla' \cdot (\nabla' V_j) \nabla'^2 V_j &= \int d^2\mathbf{r}' \frac{(\mathbf{r}-\mathbf{r}') \cdot \nabla' V_j}{|\mathbf{r}-\mathbf{r}'|^2} \nabla'^2 V_j \\
&= - \sum_{a,b} \int d^2\mathbf{r}' (\partial'_a V_j) \partial'_a \left[\frac{(r_b-r'_b)(\partial'_b V_j)}{|\mathbf{r}-\mathbf{r}'|^2} \nabla'^2 V_j \right] \\
&= \int d^2\mathbf{r}' \left\{ \frac{(\nabla' V_j)^2}{|\mathbf{r}-\mathbf{r}'|^2} - \frac{2[(\mathbf{r}-\mathbf{r}') \cdot (\nabla' V_j)]^2}{|\mathbf{r}-\mathbf{r}'|^4} - \frac{\mathbf{r}-\mathbf{r}'}{2|\mathbf{r}-\mathbf{r}'|^2} \cdot \nabla' (\nabla' V_j)^2 \right\} \\
&= \int d^2\mathbf{r}' \left\{ \frac{3(\nabla' V_j)^2}{2|\mathbf{r}-\mathbf{r}'|^2} - \frac{2[(\mathbf{r}-\mathbf{r}') \cdot (\nabla' V_j)]^2}{|\mathbf{r}-\mathbf{r}'|^4} \right\}, \tag{E9}
\end{aligned}$$

$$\int d^2\mathbf{r}' \ln|\mathbf{r}-\mathbf{r}'| \partial'_a \partial'_b (\partial'_a V_j) (\partial'_b V_j) = \int d^2\mathbf{r}' \left\{ \frac{(\nabla' V_j)^2}{|\mathbf{r}-\mathbf{r}'|^2} - \frac{2[(\mathbf{r}-\mathbf{r}') \cdot (\nabla' V_j)]^2}{|\mathbf{r}-\mathbf{r}'|^4} \right\}, \tag{E10}$$

the solution of Eq. (E8) is found to be

$$\begin{aligned}
\rho_{j,2}(\mathbf{r}) &= \frac{\rho_b \beta_{\text{eff}}^2}{2} V_j^2 - \frac{\rho_b \beta_{\text{eff}}^2 l_r^2}{8} \frac{\alpha + D_r}{\alpha + 4D_r} \nabla^2 V_j^2 + \frac{\rho_b \beta_{\text{eff}}^2 l_r^2}{16\pi} \frac{\alpha + 13D_r}{\alpha + 4D_r} \int d^2\mathbf{r}' \frac{(\nabla' V_j)^2}{|\mathbf{r}-\mathbf{r}'|^2} \\
&\quad - \frac{\rho_b \beta_{\text{eff}}^2 l_r^2}{4\pi} \frac{\alpha + 7D_r}{\alpha + 4D_r} \int d^2\mathbf{r}' \frac{[(\mathbf{r}-\mathbf{r}') \cdot (\nabla' V_j)]^2}{|\mathbf{r}-\mathbf{r}'|^4} + O\left(\frac{l_r^3}{d_j^3}\right). \tag{E11}
\end{aligned}$$

Using Eqs. (B18), (E11), and

$$\begin{aligned}
\int d^2\mathbf{r} (\nabla^2 V_j^2) \nabla V_j &= \int d^2\mathbf{r} (\nabla \cdot 2V_j \nabla V_j) \nabla V_j = -2 \sum_a \int d^2\mathbf{r} V_j (\partial_a V_j) (\nabla \partial_a V_j) \\
&= - \int d^2\mathbf{r} V_j \nabla (\nabla V_j)^2 = \int d^2\mathbf{r} (\nabla V_j)^2 \nabla V_j, \tag{E12}
\end{aligned}$$

the dipole moment is obtained as

$$\begin{aligned}
\mathbf{p}_j &= \frac{\rho_b \beta_{\text{eff}}^2 l_r^2}{8} \frac{\alpha + D_r}{\alpha + 4D_r} \int d^2\mathbf{r} (\nabla V_j)^2 \nabla V_j - \frac{\rho_b \beta_{\text{eff}}^2 l_r^2}{16\pi} \frac{\alpha + 13D_r}{\alpha + 4D_r} \int d^2\mathbf{r} (\nabla V_j) \int d^2\mathbf{r}' \frac{(\nabla' V_j)^2}{|\mathbf{r}-\mathbf{r}'|^2} \\
&\quad + \frac{\rho_b \beta_{\text{eff}}^2 l_r^2}{4\pi} \frac{\alpha + 7D_r}{\alpha + 4D_r} \int d^2\mathbf{r} (\nabla V_j) \int d^2\mathbf{r}' \frac{[(\mathbf{r}-\mathbf{r}') \cdot (\nabla' V_j)]^2}{|\mathbf{r}-\mathbf{r}'|^4} + O\left(\beta_{\text{eff}}^3 V_j^3, \frac{l_r^3}{d_j^3}\right). \tag{E13}
\end{aligned}$$

Thus the magnitude of the dipole moment satisfies

$$p_j \sim l_r^2 |\nabla V_j|_{\text{max}}^3 \tag{E14}$$

in the limit of weak potential and small run length. A numerical verification of the scaling behavior $p_j \sim |\nabla V_j|_{\text{max}}^3$ is shown in Fig. 6.

-
- [1] S. Ramaswamy, *Annu. Rev. Condens. Matter Phys.* **1**, 323 (2010).
[2] M. C. Marchetti, J. F. Joanny, S. Ramaswamy, T. B. Liverpool, J. Prost, M. Rao, and R. A. Simha, *Rev. Mod. Phys.* **85**, 1143 (2013).
[3] C. Bechinger, R. Di Leonardo, H. Löwen, C. Reichardt, G. Volpe, and G. Volpe, *Rev. Mod. Phys.* **88**, 045006 (2016).
[4] T. Vicsek, A. Czirók, E. Ben-Jacob, I. Cohen, and O. Shochet, *Phys. Rev. Lett.* **75**, 1226 (1995).

- [5] T. Vicsek and A. Zafeiris, *Phys. Rep.* **517**, 71 (2012).
- [6] J. Toner, Y. Tu, and S. Ramaswamy, *Ann. Phys.* **318**, 170 (2005).
- [7] M. E. Cates and J. Tailleur, *Annu. Rev. Condens. Matter Phys.* **6**, 219 (2015).
- [8] S. Henkes, *Phys. Rev. E* **84**, 040301 (2011).
- [9] M. Sheinman, A. Sharma, J. Alvarado, G. H. Koenderink, and F. C. MacKintosh, *Phys. Rev. Lett.* **114**, 098104 (2015).
- [10] D. Chowdhury, A. Schadschneider, and K. Nishinari, *Phys. Life Rev.* **2**, 318 (2005).
- [11] A. B. Kolomeisky and M. E. Fisher, *Annu. Rev. Phys. Chem.* **58**, 675 (2007).
- [12] F. Jülicher, K. Kruse, J. Prost, and J. Joanny, *Phys. Rep.* **449**, 3 (2007).
- [13] D. Chowdhury, *Phys. Rep.* **529**, 1 (2013).
- [14] R. Soto and R. Golestanian, *Phys. Rev. Lett.* **112**, 068301 (2014); *Phys. Rev. E* **91**, 052304 (2015).
- [15] L. Angelani and R. Di Leonardo, *New J. Phys.* **12**, 113017 (2010).
- [16] A. Kaiser, A. Peshkov, A. Sokolov, B. ten Hagen, H. Löwen, and I. S. Aranson, *Phys. Rev. Lett.* **112**, 158101 (2014).
- [17] A. Kaiser, A. Sokolov, I. S. Aranson, and H. Löwen, *Eur. Phys. J. Spec. Top.* **224**, 1275 (2015).
- [18] L. Angelani, R. Di Leonardo, and G. Ruocco, *Phys. Rev. Lett.* **102**, 048104 (2009).
- [19] A. Sokolov, M. M. Apodaca, B. A. Grzybowski, and I. S. Aranson, *Proc. Natl. Acad. Sci. USA* **107**, 969 (2010).
- [20] R. Di Leonardo, L. Angelani, D. Dell'Arciprete, G. Ruocco, V. Iebba, S. Schippa, M. P. Conte, F. Mecarini, F. De Angelis, and E. Di Fabrizio, *Proc. Natl. Acad. Sci. USA* **107**, 9541 (2010).
- [21] H. P. Zhang and H. Li, *Europhys. Lett.* **102**, 50007 (2013).
- [22] S. A. Mallory, C. Valeriani, and A. Cacciuto, *Phys. Rev. E* **90**, 032309 (2014).
- [23] W. Yan and J. F. Brady, *J. Fluid Mech.* **785** (2015).
- [24] J. Tailleur and M. E. Cates, *Europhys. Lett.* **86**, 60002 (2009).
- [25] N. Nikola, A. P. Solon, Y. Kafri, M. Kardar, J. Tailleur, and R. Voituriez, *Phys. Rev. Lett.* **117**, 098001 (2016).
- [26] C. J. O. Reichhardt and C. Reichhardt, *Annu. Rev. Condens. Matter Phys.* **8**, 51 (2017).
- [27] J. Happel and H. Brenner, *Low Reynolds number hydrodynamics: with special applications to particulate media* (Martinus Nijhoff, The Hague, 1983).
- [28] M. E. Fisher and P. G. D. Gennes, *C. R. Acad. Sci.* **287**, 207 (1978).
- [29] M. Kardar and R. Golestanian, *Rev. Mod. Phys.* **71**, 1233 (1999).
- [30] M. J. Schnitzer, *Phys. Rev. E* **48**, 2553 (1993).
- [31] F. Schweitzer, W. Ebeling, and B. Tilch, *Phys. Rev. Lett.* **80**, 5044 (1998).
- [32] P. Romanczuk, M. Bär, W. Ebeling, B. Lindner, and L. Schimansky-Geier, *Eur. Phys. J. Spec. Top.* **202**, 1 (2012).
- [33] S. A. Mallory, A. Šarić, C. Valeriani, and A. Cacciuto, *Phys. Rev. E* **89**, 052303 (2014).
- [34] X. Yang, M. L. Manning, and M. C. Marchetti, *Soft Matter* **10**, 6477 (2014).
- [35] S. C. Takatori, W. Yan, and J. F. Brady, *Phys. Rev. Lett.* **113**, 028103 (2014).
- [36] Y. Fily, A. Baskaran, and M. F. Hagan, *Soft Matter* **10**, 5609 (2014).
- [37] A. P. Solon, J. Stenhammar, R. Wittkowski, M. Kardar, Y. Kafri, M. E. Cates, and J. Tailleur, *Phys. Rev. Lett.* **114**, 198301 (2015).
- [38] F. Ginot, I. Theurkauff, D. Levis, C. Ybert, L. Bocquet, L. Berthier, and C. Cottin-Bizonne, *Phys. Rev. X* **5**, 011004 (2015).
- [39] S. C. Takatori and J. F. Brady, *Phys. Rev. E* **91**, 032117 (2015).
- [40] W. Yan and J. F. Brady, *Soft Matter* **11**, 6235 (2015).
- [41] A. P. Solon, Y. Fily, A. Baskaran, M. E. Cates, Y. Kafri, M. Kardar, and J. Tailleur, *Nat. Phys.* **11**, 673 (2015).
- [42] R. G. Winkler, A. Wysocki, and G. Gompper, *Soft Matter* **11**, 6680 (2015).
- [43] T. Speck and R. L. Jack, *Phys. Rev. E* **93**, 062605 (2016).
- [44] Y. Fily, Y. Kafri, A. P. Solon, J. Tailleur, and A. Turner, [arXiv:1704.06499 \[cond-mat.stat-mech\]](https://arxiv.org/abs/1704.06499).
- [45] C. Sandford and A. Y. Grosberg, [arXiv:1705.01610 \[cond-mat.soft\]](https://arxiv.org/abs/1705.01610).
- [46] C. Sandford, A. Y. Grosberg, and J.-F. Joanny, [arXiv:1705.01631 \[cond-mat.soft\]](https://arxiv.org/abs/1705.01631).
- [47] J. Deseigne, O. Dauchot, and H. Chaté, *Phys. Rev. Lett.* **105**, 098001 (2010).
- [48] J. Deseigne, S. Leonard, O. Dauchot, and H. Chaté, *Soft Matter* **8**, 5629 (2012).
- [49] G. Junot, G. Briand, R. Ledesma-Alonso, and O. Dauchot, *Phys. Rev. Lett.* **119**, 028002 (2017).
- [50] F. Peruani, J. Starruß, V. Jakovljevic, L. Søgaard-Andersen, A. Deutsch, and M. Bär, *Phys. Rev. Lett.* **108**, 098102 (2012).
- [51] M. E. Cates and J. Tailleur, *Europhys. Lett.* **101**, 20010 (2013).
- [52] A. P. Solon, M. E. Cates, and J. Tailleur, *Eur. Phys. J. Spec. Top.* **224**, 1231 (2015).
- [53] T. Sadhu, S. N. Majumdar, and D. Mukamel, *Phys. Rev. E* **84**, 051136 (2011).
- [54] D. Ray, C. Reichhardt, and C. J. O. Reichhardt, *Phys. Rev. E* **90**, 013019 (2014).